ELSEVIER

Polymer 42 (2001) 6247–6257

polymer

www.elsevier.nl/locate/polymer

Non-isothermal fusion bonding of polypropylene

Gregory D. Smith, Christopher J.G. Plummer, Pierre-Etienne Bourban, Jan-Anders E. Månson*

Laboratoire de Technologie des Composites et Polymères, Ecole Polytechnique Fédérale de Lausanne (EPFL), CH-1015 Lausanne, Switzerland

Received 25 August 2000; received in revised form 10 January 2001; accepted 15 January 2001

Abstract

The fusion bonding of neat polypropylene (PP) has been investigated under non-isothermal conditions with different initial adherend temperatures, and the results compared with results from bonds prepared under isothermal conditions with identical adherend temperatures. The mode I critical strain energy release rate of the bonds, G_c, was measured using a double cantilever beam geometry with a constant crack opening displacement. The effect of the adherend temperature and the hold time are summarized in time–temperature and fracture energy–temperature maps, a methodology that is easily applicable to other systems. Of immediate practical interest is the observation that for estimated interface temperatures just above the melting point, non-isothermal bonding gave bonds with G_c approaching that of the bulk resin after much shorter times than isothermal bonding.

Keywords: Fusion bonding; Polypropylene; Wedge test

1. Introduction

Many different techniques have been developed for joining thermoplastic resins and composites by fusion bonding [1–6]. They may be divided into three main categories depending on whether the heat required to provoke melting at the interface is generated by: (i) conduction from an external source, (ii) friction or electromagnetic radiation, or (iii) introduced during previous processing operations.

Category (iii) is of particular interest for multi-step injection moulding, or multi-step processing in which moulding constitutes one of the steps. It is therefore of direct concern in integrated processing (IP), a technique currently under development in our laboratory in which different polymer-based materials are combined using various processes [7–10]. Establishing strong joints between different materials, or between components with different thermo-mechanical histories is essential to the success of this approach, and is the motivation for the present work, in which we address the specific case of fusion bonds between polypropylene (PP) plaques. By varying the processing parameters we have established processing maps for non-isothermal bonding, aimed at providing guidelines for the optimization of PP bonding as part of an integrated process.

2. Experimental

2.1. Sample preparation

Shell Chemicals AG supplied a controlled rheology grade of PP with a narrow molecular weight distribution, designated VM6100H, in the form of extruded pellets. Differential scanning calorimetry (DSC) heating scans of 5 mg samples at 10 K min^{-1} indicated the peak temperature of the melting endotherm of the as-received resin to be 165°C. We henceforth refer to this as the melting point, T_m. The recrystallization exotherm observed during cooling at the same rate started at about 123°C and peaked at 110°C. 50×50 mm^2 square plaques with a thickness of about 2 mm were prepared by injection moulding. (Melt temperature, 195°C; injection pressure, 60 MPa; mould temperature, 100°C.)

The plaques were bonded using an instrumented matched-die mould installed on a servo-hydraulic load frame, shown schematically in Fig. 1. The temperatures of the upper (T_1) and lower (T_2) halves of the mould were controlled separately, and recorded as a function of time using thermocouples located on the upper and lower mould faces. A plaque was placed in the upper mould and after T_1 and T_2 had stabilized to within 1 K of the required values, a second plaque was placed in the lower mould and covered with an insulating sheet. The system was allowed to equilibrate for $t_{eq} = 10$ min, after which the insulating sheet was removed, the mould closed and a pressure p applied. After

* Corresponding author. Tel.: +41-21-693-4281; fax: +41-21-693-5880.
E-mail address: jan-anders.manson@epfl.ch (J.-A.E. Månson).

0032-3861/01/$ - see front matter
PII: S0032-3861(01)00060-X

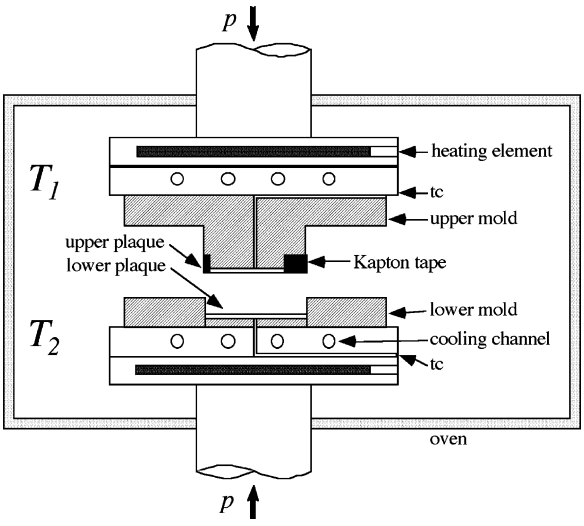

Fig. 1. Schematic of the $50 \times 50\ mm^2$ matched-die mould showing the heating elements, cooling channels and thermocouples (tc) located at the upper and lower mould faces.

a hold time t_{hold}, the heaters and oven were turned off, but the pressure was maintained during subsequent cooling to 30°C. The initial cooling rate was about 55 K min^{-1} in each case.

Two series of bonds, A1 and A2, were initially prepared in order to compare the effects of isothermal and non-isothermal conditions. Their processing parameters are listed in Table 1. For the isothermal series A1 the hold time was 600 s, whereas a hold time of 42 s was chosen for the non-isothermal series A2. In each case we took the initial interface temperature, T_i, to equal the mean of the plaque temperatures prior to bonding, $(T_1 + T_2)/2$. The validity of this assumption has been demonstrated elsewhere using a one dimensional heat transfer model and direct measurements of the interface temperature during bonding [11].

Four additional series of bonds, B1–B4, were prepared in order to investigate further the influence of the processing parameters, which are again listed in Table 1 for each series. For these bonds, the mould was enclosed in an oven and the temperature maintained at 2°C below T_1 to improve the uniformity of the plaque temperatures.

2.2. Fracture testing

The mode I fracture energy of the bonds was measured using the double cantilever beam geometry with a constant crack opening displacement, also known as the 'wedge test' and shown in Fig. 2a. Approximately $4 \times 10 \times 50\ mm^3$ bars were machined from the centre of the bonded specimens. A notch was introduced at the interface prior to bonding by inserting a layer of Kapton tape between the plaques along one edge. Crack propagation was induced by driving a 0.46-mm thick wedge into the notch and along the interface at a speed of 2 mm min^{-1} using a screw driven load frame. The position of the crack tip was recorded using a video camera as shown in Fig. 2b.

Table 1
Processing parameters for the PP/PP bonds ($\Delta T = T_2 - T_1$)

Series	T_1 (°C)	T_2 (°C)	t_{hold} (s)	p (MPa)	T_i (°C)	ΔT (°C)
A1	100–160	100–160	600	2	100–160	0
A2	100–160	200	42	2	150–180	100–40
B1	120–170	200	40	2	160–185	80–30
B2	167–110	173–230	40	2	170	6–120
B3	140	200	0–600	2	170	60
B4	140	200	40	0–40	170	60

G_c was calculated using Kanninen's expression [12,13]

$$G_c = \frac{3\Delta^2 E h_1^3 h_2^3}{8a^4}\left(\frac{h_1^3 C_2^2 + h_1^3 C_1^2}{(h_1^3 C_2^3 + h_2^3 C_1^3)^2}\right), \quad (1)$$

where $C_1 = 1 + 0.64h_1/a$, $C_2 = 1 + 0.64h_2/a$, Δ the wedge thickness, E the Young's modulus, h the beam thickness and the subscripts 1 and 2 refer to the upper and lower beams, respectively. Since PP is viscoelastic, E should be considered to be time dependent [14]. The time available for relaxation of stress in a volume element ahead of the crack tip is approximately

$$\delta t = \frac{a}{\dot{a}},$$

where a is the crack length and $\dot{a}$ is the crack propagation velocity. E was accordingly measured in three-point bending at a frequency of 0.016 Hz, which is of the order of $1/\delta t$ for the crack speeds considered here, giving a value of 1.71 GPa.

2.3. Microscopy

The fracture surfaces were coated with Au/Pd and examined using a JEOL JSM-6300F scanning electron microscope (SEM). The through-thickness morphology of the specimens was characterized by optical microscopy (OM) of roughly 10-μm thick microtomed sections. For more detailed investigation of the lamellar morphology of well

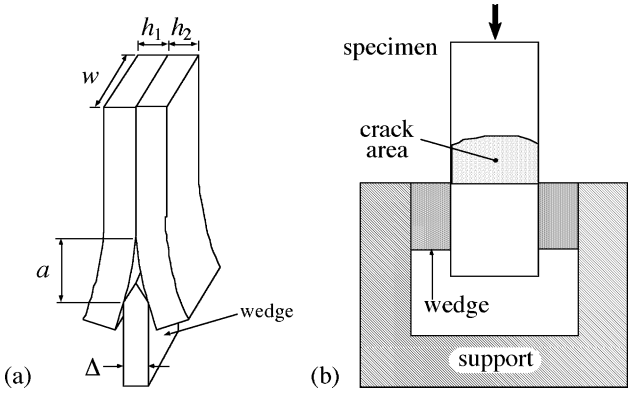

Fig. 2. The double cantilever beam geometry with a constant crack opening displacement: (a) specimen geometry; (b) measurement of the crack length.

bonded interfaces we also made use of transmission electron microscopy (TEM) of carbon replicas of internal surfaces. After they had been exposed and smoothed with a glass knife, these surfaces were etched following the method of Olley [15]. C/Pt shadowed two-stage carbon replicas were then prepared as described elsewhere [16] and observed using a Philips EM430ST TEM at 300 kV.

3. Results

3.1. Bond strengths

G_c for the isothermal bonds A1 is plotted as a function of T_i in Figs. 3a,c. For T_i at and below T_m, where little melting of the plaques was expected to occur, G_c was relatively low, ranging from 16 J m^{-2} at $T_i = 150$°C to 35 J m^{-2} at $T_i = T_m$. As T_i increased above T_m, however, G_c increased sharply, reaching a value of 5.8 kJ m^{-2} at $T_i = 180$°C, which corresponds to the G_c of the bulk polymer.

G_c for the non-isothermal bonds A2 and B1 is plotted as a function of T_i in Figs. 3b,c. In spite of the slightly different processing conditions, the two data sets were very similar. For T_i well below T_m, G_c was about 200 J m^{-2} in each case, which represented a tenfold improvement over the isothermal bonds as illustrated in Fig. 3c. At higher temperatures, G_c increased monotonically with T_i, reaching between 4 and 5 kJ m^{-2} at 180°C, that is, slightly less than in isothermal bonding with the same interface temperature.

Results for the non-isothermal bonds B2 are shown in Fig. 3d. In this case, T_i was kept constant at 170°C and the temperature difference between the solid and molten plaques, ΔT, was varied. For ΔT greater than about 10 K, the upper plaque did not melt (since $T_l = T_i - \Delta T/2$). In this regime, G_c increased with ΔT, reaching about 870 J m^{-2} at $\Delta T = 60$°C. At the highest ΔT however, the scatter in G_c became too large for a clear trend to be identifiable. This has been linked to thermal degradation, whose extent varies considerably with position within the plaques as a consequence of the different local thermal history and degree of molecular orientation [11].

The effect of t_{hold} on non-isothermal bonds is shown Fig. 4a for $T_i = 170$°C. For t_{hold} up to about 40 s, G_c remained roughly constant at 900 J m^{-2}, this value apparently being reached vary rapidly once initial

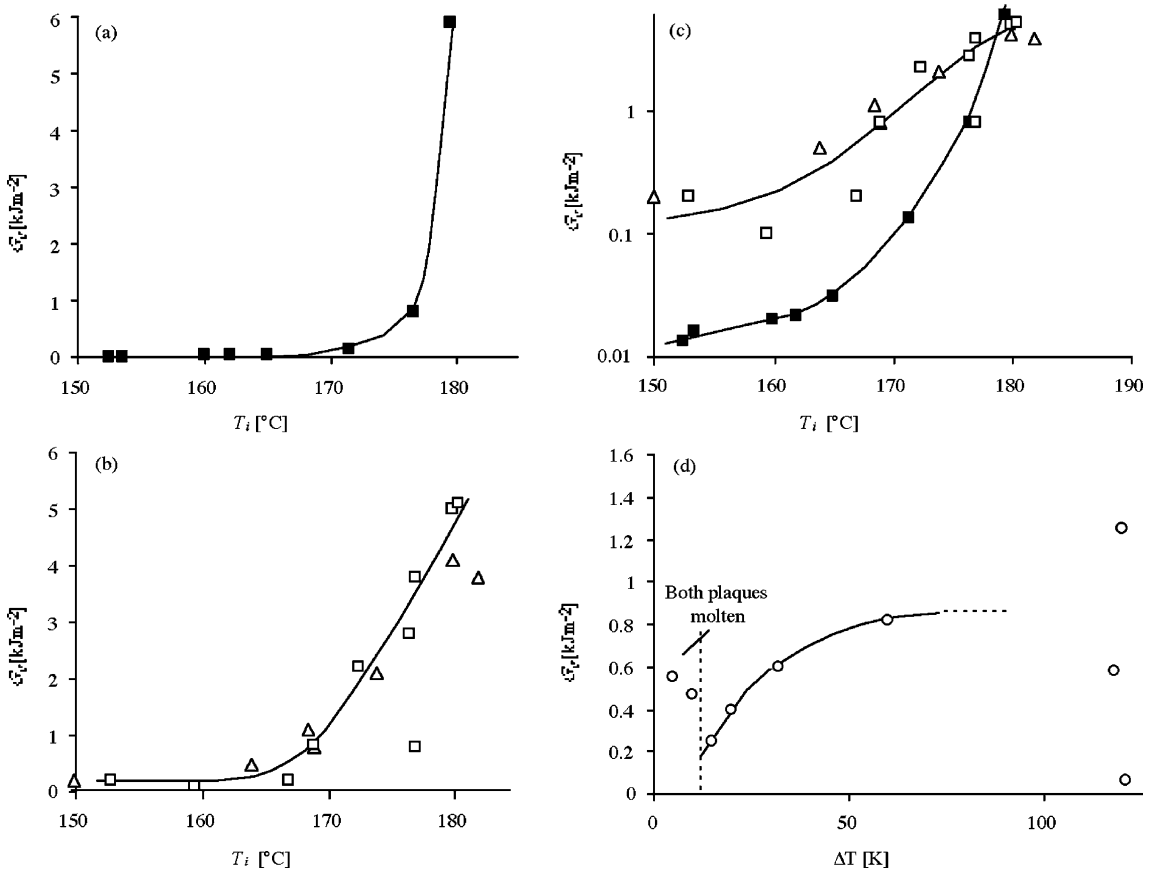

Fig. 3. (a) G_c as a function of T_i for the isothermal bonds A1 ($t_{hold} = 600$ s, $p = 2$ MPa); (b) G_c as a function of T_i for the non-isothermal bonds A2 (triangles) and B1(squares) ($t_{hold} = 40$ and 42 s, $p = 2$ MPa); (c) comparison of the data for A1, A2 and B1 on a log-linear plot (symbols as previously in Figs. 3a,b); (d) G_c as a function of ΔT for the non-isothermal bonds B2 ($T_i = 170$°C, $t_{hold} = 40$ s, $p = 2$ MPa).

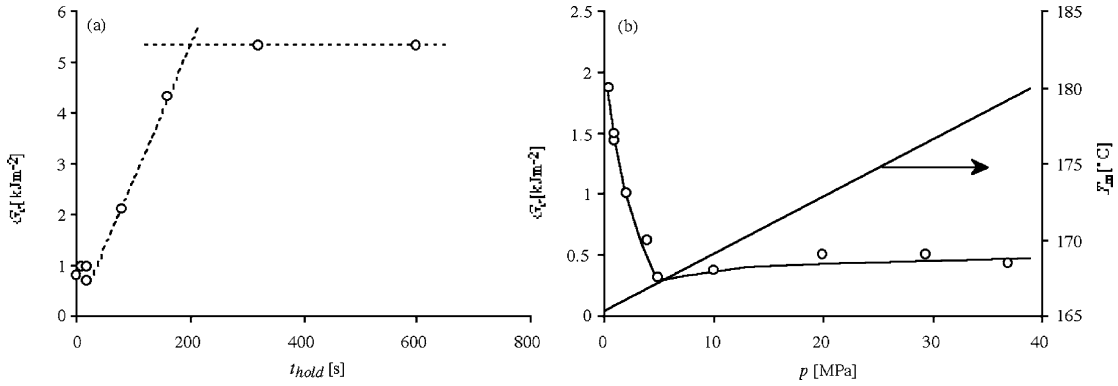

Fig. 4. (a) G_c as a function of t_{hold} for the non-isothermal bonds B3 ($T_i = 170°C$, $p = 2$ MPa); (b) G_c and T_m as a function of $p$for the non-isothermal bonds B4 ($T_i = 170°C$, $T_1 = 140°C$).

contact was established between the two plaques. As t_{hold} was increased further, G_c began to increase more strongly, reaching 5.3 kJ m^{-2} at 320 s. At $t_{hold} = 600$ s, however, G_c showed no further increase, suggesting 5.3 kJ m^{-2} to be close to the value for bulk PP. This compares with G_c values of about 100 J m^{-2} after 600 s of isothermal bonding at 170°C.

G_c is shown as a function of p for $T_i = 170°C$ and $T_1 = 140°C$ in Fig. 4b. There were two distinct regimes of behaviours: (i) a low pressure region where G_c decreased with p, falling from approximately 1500 J m^{-2} at 0.5 MPa to 300 J m^{-2} at 5 MPa; (ii) a higher pressure regime where G_c was about 500 J m^{-2}, and weakly dependent on p. These results may to some extent be accounted for by the observation that T_m in PP increases linearly with p by 0.38 K MPa^{-1} in the relevant pressure range [17]. The pressure at which $T_m(p) = T_i = 170°C$ represents the highest pressure at which the surface of the plaque initially at 140°C was able to melt. This is consistent with Fig. 4b in so far as there was a sharp increase in bond strengths for low p, although the threshold was somewhat less than the estimated value of 11 MPa.

3.2. Morphology and fractography

The striated surface texture of as-moulded plaques, shown Fig. 5a, was assumed to be due to the texture of the mould walls. The sub-surface morphology is shown Fig. 5b. Towards the interior of the plaque there were signs of shear-induced structure. However, the most obvious morphological feature of Fig. 5b is the columnar zone adjacent to the surface. Such zones are typical of mouldings where rapid external cooling leads to a high surface nucleation density and strong thermal gradients immediately behind the surface [18,19]. The plaques were also observed to shrink along the original flow direction on re-melting, which indicated a certain amount of flow induced orientation [11].

The fracture surfaces of isothermal and non-isothermal bonds with $T_i = 160°C$ are shown in Figs. 6a,b. Crack propagation was from left to right in these and in all subsequent SEM micrographs of the fracture surfaces. The fracture surface texture of the bond made under isothermal conditions was similar to that of the un-bonded sample in Fig. 5a. This is not surprising, given that at 160°C both sides

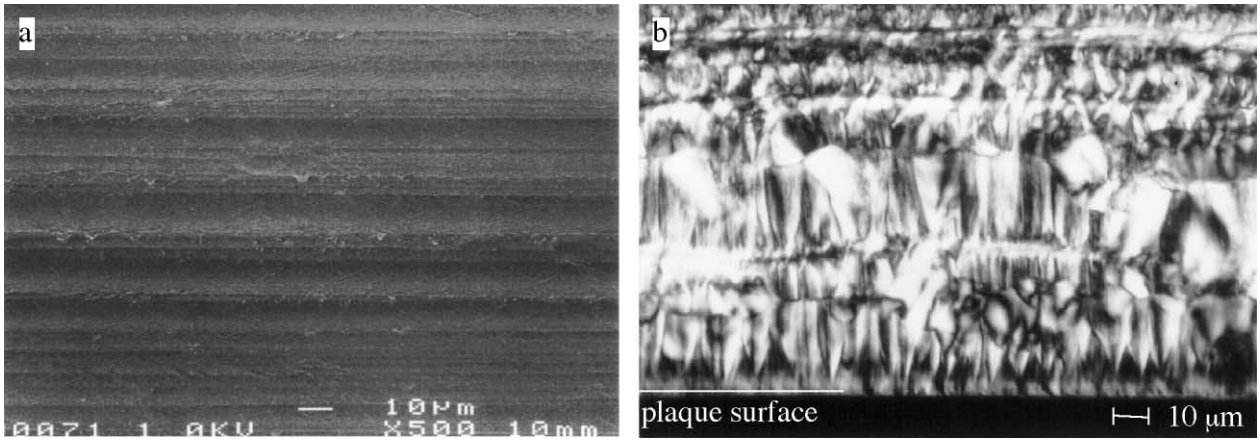

Fig. 5. (a) SEM of the surface texture of an as-moulded plaque; (b) OM of a thin transverse section through the surface viewed between crossed polarizers.

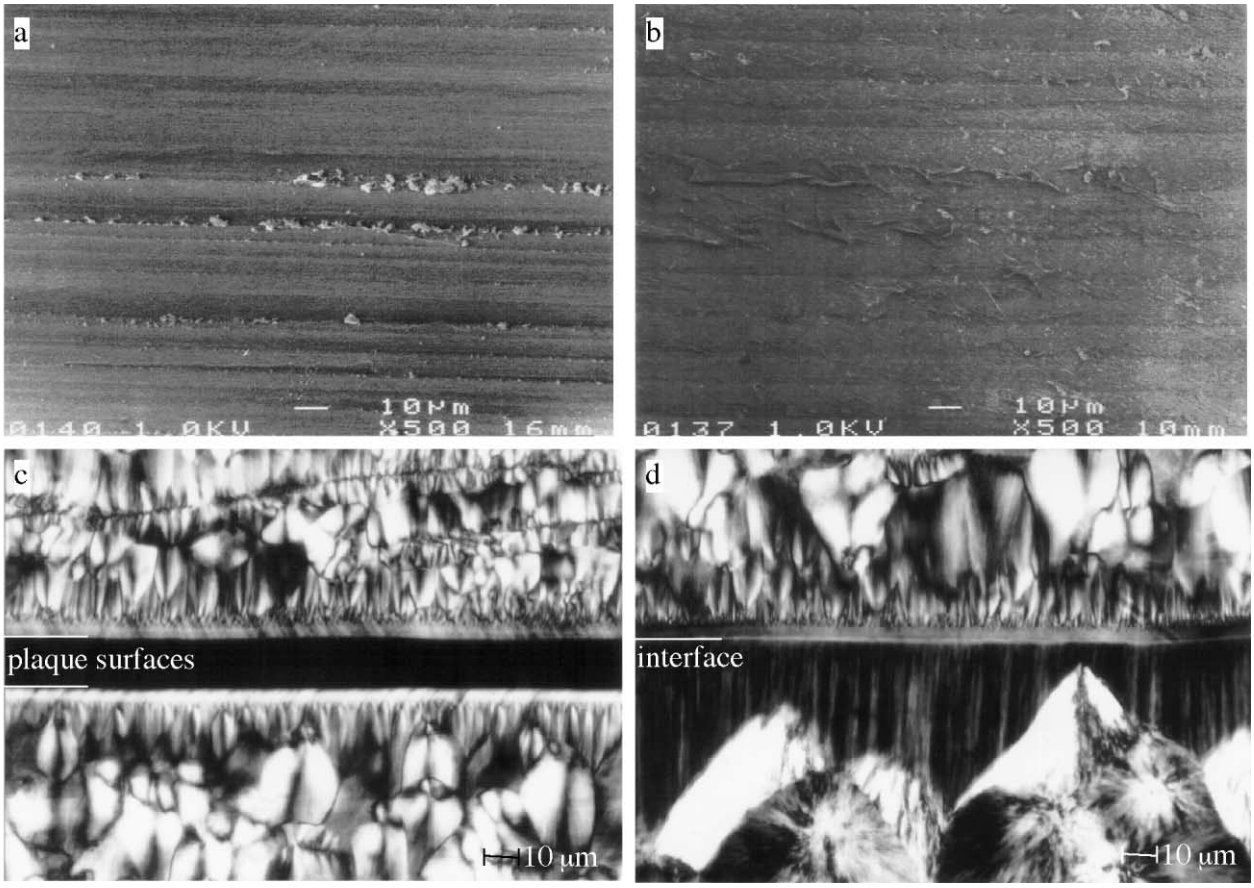

Fig. 6. (a) SEM of the fracture surface of a specimen bonded isothermally at 160°C; (b) SEM of the fracture surface of a specimen bonded non-isothermally with $T_i = 160$°C and $T_1 = 120$°C; (c) OM of a thin transverse section through the bond made under isothermal conditions, viewed between crossed polarizers; (d) OM of a thin transverse section through the bond made under non-isothermal conditions, viewed between crossed polarizers.

of the interface were below T_m. The lack of extensive plastic deformation was also anticipated from the low values of G_c observed for these bonds, which generally failed during sectioning as shown in Fig. 6c. Comparison of Fig. 6c with Fig. 5b again indicates little change in the sub-surface microstructure during isothermal bonding. This was also true of the upper (solid) plaque after non-isothermal bonding (Fig. 6b). On the other hand, the morphology of the lower (initially molten) plaque was substantially altered as shown in Fig. 6d. The equilibration time of 10 min at 200°C was sufficient to provoke a significant reduction in nucleation density in the interior of the plaque, although a columnar region was still present at the interface, presumably owing to contact with the cold plaque during cooling. Also visible in Fig. 6d are a number of β-phase spherulites, which had nucleated behind the (mainly α-phase) columnar region.

The fracture surfaces of the upper plaques of the bonds with $T_i = 170$°C, are shown in Figs. 7a,b. The original surface texture was still apparent in the isothermal case, showing little melting to have taken place, although $170°C > T_m$. There was some evidence for localized deformation associated with the striations, but the lack of texture elsewhere suggested that intimate contact was not established over the whole of the interface. In the case of non-isothermal bonding, however, the original surface texture of the upper plaque was strongly modified, suggesting the surface to have undergone substantial melting and/or deformation. As shown in Fig. 7b a series of ridges of material oriented at approximately 55° to the direction of crack propagation were visible on the fracture surface. Closer examination also revealed cracks or crazes growing in the direction of propagation from the depressions between these ridges, inclined at an angle of about 20° to the plane of the interface [11].

The cross-sections of the bonds are shown in Figs. 7c,d. In the isothermal case, the original columnar morphology was strongly tilted on either side of the interface, reflecting substantial shear of the partly molten material during bonding [20]. The texture of the columnar regions was also altered, the original structure having undergone substantial recrystallization to give a much finer texture. Shear of the columnar zone is again visible in the upper plaque in Fig. 7d, but in this case the structure of the lower plaque was similar to that in Fig. 6d. Fig. 8 shows the same interface as in Fig. 7d, but in the vicinity of the pre-notch where the Kapton tape is visible. This micrograph confirms the origin of the columnar region in the lower plaque to be direct contact with the surface of the upper plaque, since the nucleation

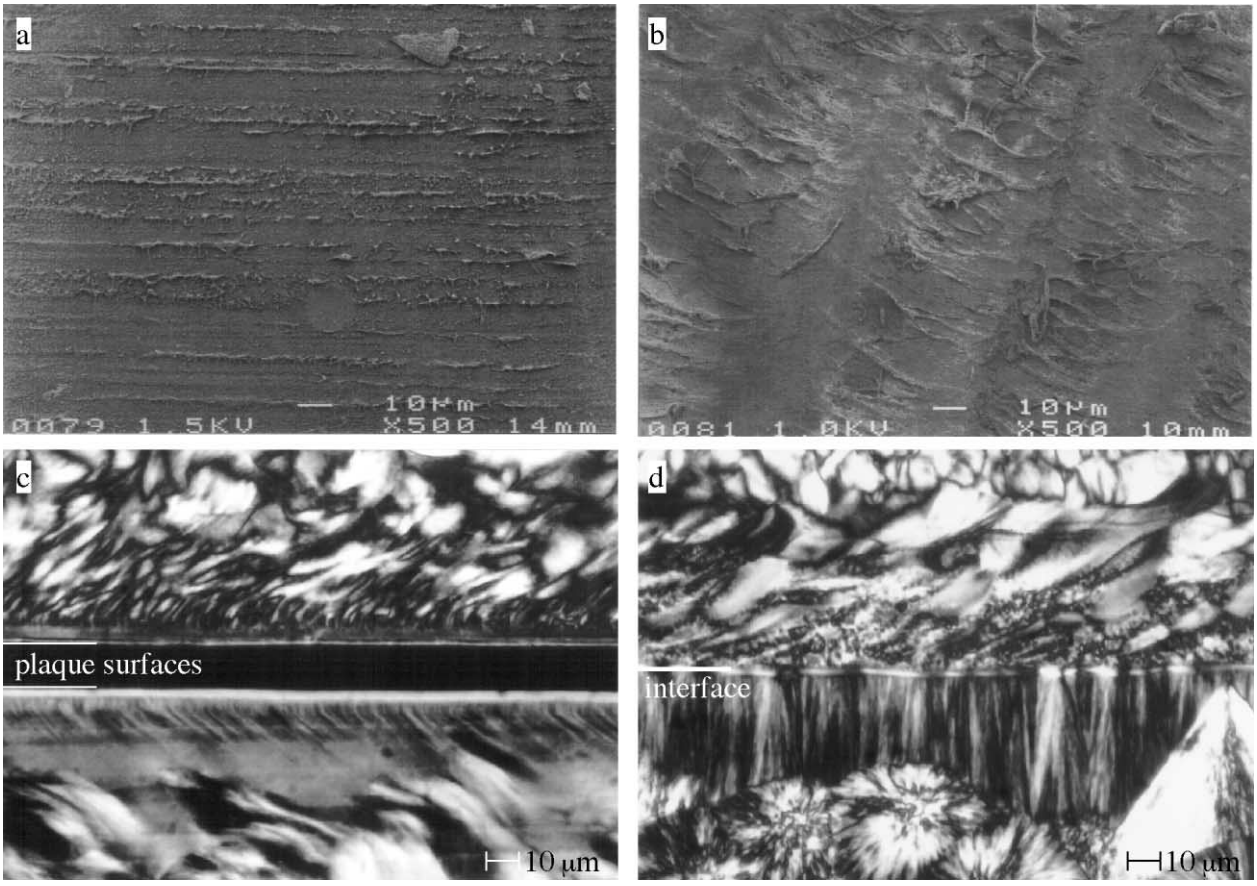

Fig. 7. (a) SEM of the fracture surface of a specimen bonded isothermally at 170°C; (b) SEM of the fracture surface of a specimen bonded non-isothermally with $T_i = 170$°C and $T_1 = 140$°C; (c) OM of a thin transverse section through the bond made under isothermal conditions, viewed between crossed polarizers; (d) OM of a thin transverse section through the bond made under non-isothermal conditions, viewed between crossed polarizers.

density in the former was much reduced where it was in contact with the Kapton.

Fracture surfaces for bonds with $T_i = 180$°C are shown in Figs. 9a,b. At this temperature the original surface texture was erased under both isothermal and non-isothermal conditions. Indeed, the fracture surfaces was similar, although the fracture surface for non-isothermal bonding appeared slightly rougher. Bonding in both cases significantly altered the sub-surface structure, shown in Figs. 9c,d. Regions of columnar growth still marked the position of the original interface, but were interspersed with regions in which no columnar growth was visible. These regions were somewhat more extensive for isothermal bonding.

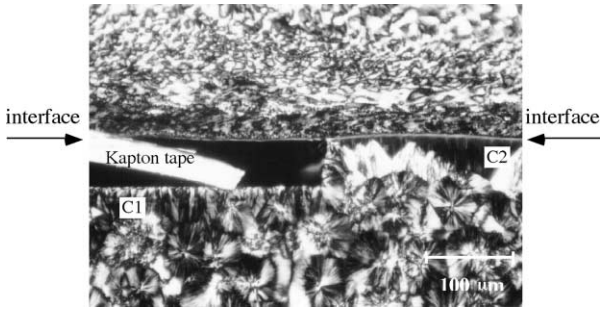

Fig. 8. OM of a thin transverse section through the pre-crack in a bond made under non-isothermal conditions ($T_i = 180$°C and $T_1 = 140$°C).

A TEM micrograph of a replica from the interfacial region of the bond made under isothermal conditions at 180°C is shown in Fig. 10a. As in the optical micrograph, α-phase columnar regions are visible adjacent to the interface, as well as occasional β-phase spherulites as indicated in the figure, identifiable from their relatively coarse lamellar texture [21]. The detail shown in Fig. 10b shows some continuity of the lamellar structure across the original interface locally, although the interface is still clearly visible in other parts of the specimen, suggesting a non-uniform contact and/or a non-uniform interface temperature.

The fracture surfaces of the upper plaques from three bonds with different hold times and $T_i = 170$°C are compared in Fig. 11. The location of the micrographs on the upper plaque surface is shown schematically in Fig. 11a with respect to the melt flow during filling. The fracture surface shown in Fig. 11b was for a bond prepared under the same conditions as that in Fig. 7b and shows essentially the same features. Comparison with Fig. 11a indicates the characteristic ridged structure to be roughly tangential to the melt front in this case. For the bond made with $t_{hold} = 80$ s, similar patterns of ridges and troughs were again present,

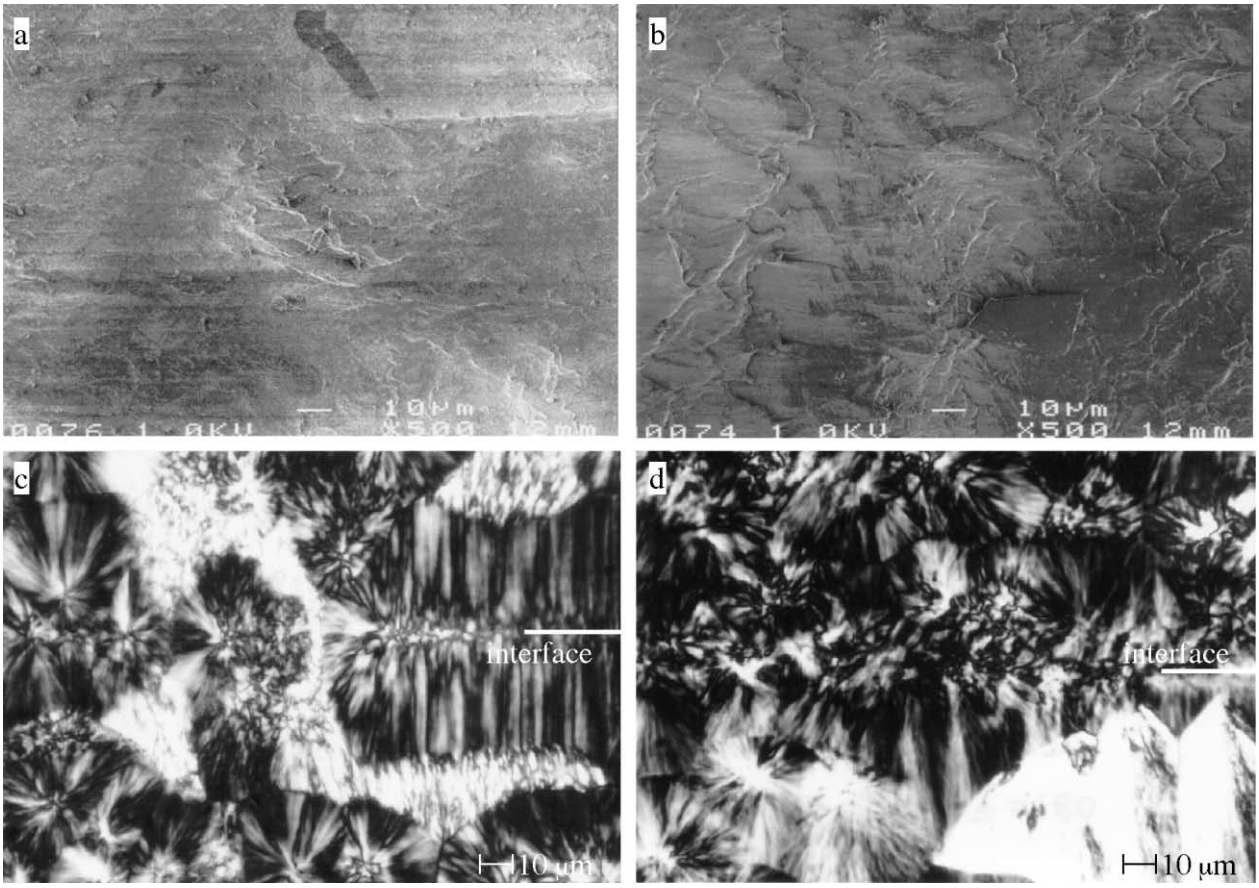

Fig. 9. (a) SEM of the fracture surface of a specimen bonded isothermally at 180°C; (b) SEM of the fracture surface of a specimen bonded non-isothermally with $T_i = 180$°C and $T_1 = 160$°C; (c) OM of a thin transverse section through the through the bond made under isothermal conditions, viewed between crossed polarizers; (d) OM of a thin transverse section through the bond made under non-isothermal conditions, viewed between crossed polarizers.

but regions of more extensive plastic deformation were also visible, as shown in Fig. 11c. The failure in the region immediately above the centre of the micrograph was localized in the upper plaque, whereas that in the larger region in the lower left-hand part of the micrograph was associated with the lower plaque. The fracture surface of the bond with $t_{hold} = 320$ s (Fig. 11d), showed no ridges or troughs, and failure occurred in the lower plaque. Secondary cracks perpendicular to the direction of propagation were also visible in this case.

4. Discussion

The results presented in the Section 3 were broadly consistent with the anticipated trends, raising the interface temperature and hold time resulting in increased bond strengths, particularly when the interface temperature was above T_m. However the observation that non-isothermal bonding gave stronger interfaces after shorter times than isothermal bonding for T_i below and immediately above T_m was less expected. It is also of immediate technological interest, particularly for the processing techniques referred to in the introduction. It shows that it is not necessary to reheat the interface of given component to well above its melting point in order to obtain optimized bonding with a second, initially molten component. Moreover it is not necessary to heat the molten component to excessively high temperatures in order to compensate for the low temperature of the solid component. Indeed, for the melt temperature of 200°C used here, useful bond strengths (G_c of a few 100 J m^{-2}) were obtained very rapidly, even when the interface temperature was well below the melting point.

One possible contributing factor to these observations was that T_i, as we defined it, was not a good measure of the interface temperature during bonding. This is partly borne out by the observed increase in G_c with ΔT for fixed T_i. A simple explanation for this is that the heat capacity of PP is an increasing function of T, and that its rate of increase with Tincreases sharply above T_m [22]. Thus if the non-isothermal interfaces had been allowed to equilibrate under adiabatic conditions after contact, the final temperature would have been greater than T_i. By extension, larger ΔT might be expected to lead to interface temperatures greater than $(T_1 + T_2)/2$, particularly in the earlier stages of bonding where the thermal gradients close to the interface are expected to be large.

However, this does not satisfactorily explain the

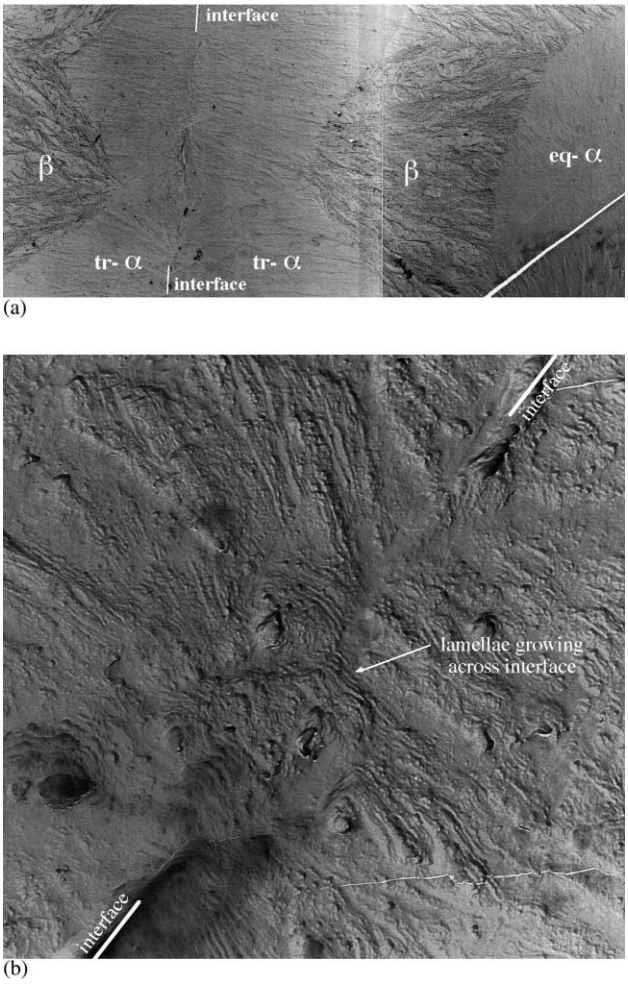

Fig. 10. TEM of a replica from a section through the interface.

invariance of G_c at T_i well below T_m, where examination of the fracture surfaces confirmed little melting to have taken place at the surface of the solid plaque, even where ΔT was large. Similarly, changing T_m by changing the applied pressure had little influence at fixed ΔT when $T_i < T_m$, G_c remaining of the order of 100 J m^{-2}. Consideration of the micrographs suggested the low G_c values for the isothermal bonds to have resulted from poor contact and wetting at the interface during bond formation. It is therefore inferred that the superior properties of the non-isothermal bonds in this regime were at least partly due to efficient wetting of the interface by the molten plaque. This was reflected by the fact that the solid plaque provoked columnar growth in the molten plaque on cooling, suggesting a certain degree of self-epitaxy, or at the very least, intimate contact across the interface.

Since there was little apparent plastic deformation at the fracture surface of the solid plaques for $T_i < T_m$, it might further be inferred that the bond strength in the non-isothermal case was primarily due to secondary interactions across the interface, as opposed to inter-diffusion. The surface energy of PP is about 30 mJ m^{-2} [23] (or possibly greater in this case owing to surface orientation and transcrystallinity) which would lead to negligible values of G_c if interface failure were by simple cleavage. However, given an inter-chain separation of the order of 0.4 nm, it also implies a joint strength in tension of about 100 MPa in the absence of flaws or other defects [24], which would be largely sufficient to provoke plastic deformation in the material immediately adjacent to the interface, resulting in the additional dissipation necessary to account for the observed G_c. Final rupture would nevertheless be expected to occur at the interface, whose ultimate tensile strength would remain much less than that for failure of the bulk polymer.

At an interface temperature of 170°C, the ridged structure of the fracture surfaces of the solid plaques was indicative of a substantial amount of structural relaxation at the surface of these latter [18]. This was borne out by the orientation of the ridges with respect to the original flow direction during injection moulding shown in Fig. 11. For short t_{hold} and/or interface temperatures just above T_m, the extent of plastic deformation at the fracture surface remained limited. However, as t_{hold} and/or T_i were increased, plastic deformation became widespread, intermediate G_c being characterized by mixed fracture surfaces.

In considering these results, it should be recognized that by identifying T_m with the peak of the melting endotherm in a DSC run, one ignores the fact that the effective local melting point varies significantly in semicrystalline polymers [25]. This is particularly true of the surface of injection mouldings, where the oriented structure associated with the skin layers may show memory effects even after T has exceeded the equilibrium melting point of the resin [26,27]. Therefore the kinetics and temperature dependence of the build up of strength during fusion bonding of a semicrystalline polymer just above T_m may not be simply related to self-diffusion in the melt, contrary to what is usually assumed in the healing of amorphous polymers, for example [28]. Indeed the TEM micrographs and the fracture surfaces indicate strong bonding to be associated with the establishment of a continuous lamellar texture across the interface, which would be contingent on full melting and the erasure of memory effects. This need not imply that co-crystallization itself is sufficient for strong bonding, since it would be a natural consequence of the establishment of an inter-diffused, relaxed melt structure at the interface during bonding. Bearing in mind the important role of the skin layer in this respect, it would be interesting to look at the effects of different surface textures, and more particularly, the effect of machining away the highly persistent oriented layers at the surface of the injection mouldings used here.

4.1. Processing windows

As stated in the introduction, one of the aims of the present work has been to establish processing windows for non-isothermal fusion bonding in PP, based on the results of

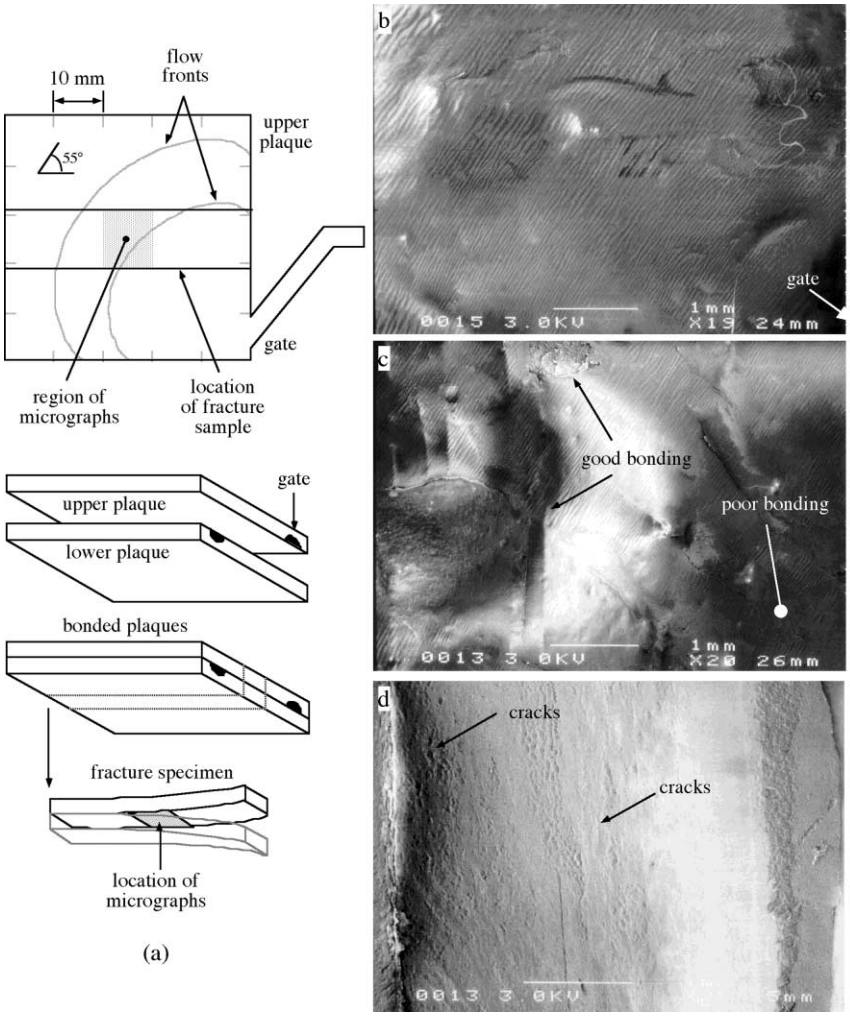

Fig. 11. Fracture surfaces for different hold times: (a) location of the micrographs on the upper plaque surface with respect to the melt flow front during filling; (b) fracture surface for $t_{hold} = 40$ s; (c) fracture surface for $t_{hold} = 80$ s; (d) fracture surface for $t_{hold} = 320$ s.

the tests. These are summarized in Fig. 12 for the specific case of $T_2 = 200°C$. In the processing diagram in time–temperature space shown in Fig. 12a, $T_i < T_m$ defines a regime in which bonding is assumed to be essentially adhesive as discussed in the Section 4. On the other hand, a value of G_{Ic} assumed to be close to that of bulk PP, was obtained at $T_i = 180°C$ after 42 s and this was taken to define a regime of optimum bonding as indicated in the Fig. 12a. From series B3, the time required to achieve optimum bonding for $T_i = 170°C$ was approximately 200 s. The stability of the polymer limits the time the melt can be held in contact with air. Based on thermal gravimetric analysis measurements of the degradation time in oxygen of the as-received resin [11] we express the isothermal degradation time as

$$t_{deg}^{iso} = \frac{1}{A\exp(-E_a/RT)} \quad (2)$$

where E_a is approximately 130 kJ mol^{-1} and $A = 1.265 \times 10^{11}$ s^{-1} (consistent with values reported elsewhere [29,30]). The onset of degradation measured for the injection moulded plaques by DSC was found to be significantly shorter than given by Eq. (2), reflecting the processing induced degradation referred to earlier. On the other hand, Billingham et al. showed the degradation time to be inversely proportional to the square root of the partial pressure of oxygen [29], so that in air t_{deg}^{iso} should be 2.2 times longer than t_{deg}^{iso} in oxygen. To take these effects into account in Fig. 12a, the degradation times were re-scaled to be consistent with the DSC data, and multiplied by 2.2. For the purposes of calculating the time–temperature window corresponding to thermal degradation, the same temperature dependence was assumed as in Eq. (2). More generally the onset of degradation will depend on the specific thermo-mechanical history of the samples, residual stress [31], the nature of the additive package [32], the molar mass [33] and so forth, so the degradation windows shown in Fig. 12 should only be taken to be indicative.

A second processing window for non-isothermal bonding was constructed in G_{Ic}–ΔT space as shown in Fig. 12b. G_{Ic} as a function of ΔT for series B2 was fitted

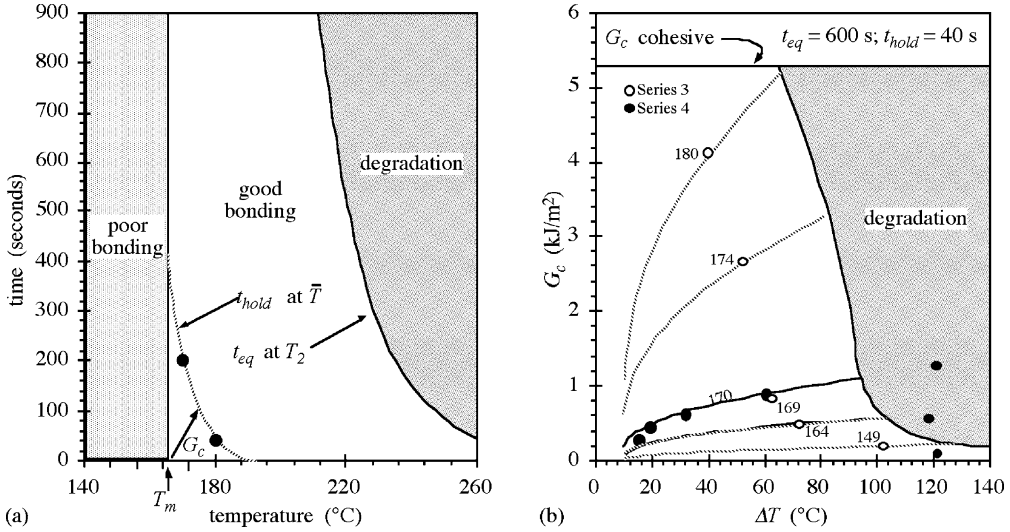

Fig. 12. Processing windows for non-isothermal bonds: (a) in time–temperature space; (b) in G_c–ΔT space.

to the parabolic expression

$$G_{Ic} = \left(\frac{\Delta T - \Delta T_o}{\xi}\right)^{1/2} + G_{Ic}^{o}, \quad (3)$$

where ξ was 100 $Km^4 J^{-2}$. The remainder of the diagram was constructed assuming the curves for other values of T_i to differ only in the value of ξ. Appropriate values of ξ were then derived from the results of series B2, and used to calculate the dashed lines in Fig. 12b. The region where degradation of the resin occurs was calculated as in Fig. 12a.

5. Conclusion

For estimated interface temperatures just above the melting point, non-isothermal bonding between a solid PP plaque and a plaque initially at 200°C has been shown to result in bonds with G_c approaching that of the bulk resins. This occurred after much shorter times than isothermal bonding at the same interface temperature. Moreover, even for interface temperatures below the melting point, non-isothermal bonding resulted in adhesive bonds with G_c of the order of 100 $J m^{-2}$, whereas the isothermal bonds had negligible strength. Thus, although our interest in non-isothermal bonding stems mainly from its relevance to multistep processing, the present work suggests that it may be intrinsically advantageous with respect to isothermal bonding in terms of processing times and temperatures.

Based on the results, outlines have been given for processing windows that delineate regions of weak bonding from those where G_c is comparable with that in bulk PP. They show that considerable freedom in the choice of adherend temperatures is possible in the present case since the degradation of the polymer does not occur until much higher temperatures or longer times than required for bonding. Although this may not be the case for more sensitive resins, the method used here can be easily applied to other systems.

Acknowledgements

We would like to thank the Swiss Priority Program on Materials Research (PPM) for their financial support and Brian Senior of the EPFL-CIME for his help with the SEM.

References

[1] Benatar A, Gutowski TG. SAMPE J 1986;19:33.
[2] Bourban PE, Gillespie JW, Tierney JT. Joining of composites. In: Kelly A, Zweben C, editors. Comprehensive composite materials. Amsterdam, New York: Elsevier, Pergamon, 2000.
[3] Grimm RA. Adv Mater Proces 1995;3:27.
[4] Potente H, Natrop J, Pederson TK, Uebbing M. J Therm Compos 1993;6:147.
[5] von der Ohn J. Weld Int 1990;4:288.
[6] Weber J. Weld J 1990;69:52.
[7] Bourban PE, Bonjour F, Månson JAE. In: Proceedings ECCM7. London, UK, May 14–16, 1996;201.
[8] Bourban PE, Bögli A, Bonjour F, Månson JAE. Compos Sci Technol 1998;58:633–7.
[9] Wakeman MD, Bourban PE, Bonjour F, Månson JAE. In: Proceedings of SAMPE-ACCE-DOE, 1999.
[10] Bourban PE, Bonjour F, Bernet N, Wakeman MD, Månson JAE. In: Proceedings ICCM12, Paris, paper 595, 1999.
[11] Smith GD. PhD Thesis 1597. Ecole Polytechnique Fédérale de Lausanne, 1997.
[12] Kanninen MK, Int. J Fract 1973;9:83.
[13] Creton C, Kramer EJ, Hui CY, Brown HR. Macromolecules 1992;25:3075.
[14] de Gennes PG, C R. Acad Sci Paris 1988;307(II):1949.
[15] Olley RH, Bassett DC. Polym Commun 1982;23:1707.
[16] Sawyer LC, Grubb DT. Polymer microscopy. London: Chapman and Hall, 1987.
[17] Leute U, Dollhop W, Liska E. Colloid Polym Sci 1978;256:914.
[18] Fujiyama M. Higher order structure of injection-molded polypropylene. Polypropylene: structure, blends and composites. 1995. p. 167.
[19] Keller A, Manchin J. J Macromol Sci 1967;B1:41.
[20] Oliveira MJ, Hemsley DA. British Polym J 1985;17:269.
[21] Olley RH, Bassett DC. Polymer 1989;30:399.
[22] Gaur B, Wunderlich B. J Phys Chem Ref Data 1981;10:1051.

[23] Wu S. Polymer interface and adhesion. New York: Marcel Dekker, 1982.
[24] Kinloch AJ. Adhesion and adhesives. New York: Chapman and Hall, 1987.
[25] Wunderlich B. Macromolecular physics, vols. 1–3. New York: Academic Press, 1980.
[26] Fujiyama M, Wakino T. J Appl Polym Sci 1988;35:29.
[27] Varga J. Angew Makromol Chem 1983;112:191.
[28] Kausch HH. Polymer fracture. 2nd ed. Berlin: Springer, 1987.
[29] Billingham NC, Bott DC. Developments in polymer degradation. New York: Applied Science, 1981. p. 63.
[30] Oswald HJ, Turi E. Polym Eng Sci 1965;5:152.
[31] Czern J. J Appl Polym Sci 1972;16:2623.
[32] Gugumus F. Polym Degrad Stab 1994;44:299.
[33] Gensler R, Plummer CJG, Kausch HH, Kramer E, Pauquet JR, Zweifel H. Polym Degrad Stab 2000;67:195.